



Coherence of Ion Cyclotron Resonance in Damped Ion Cyclotron Waves in Space Plasmas

Qiaowen Luo^{1,2}, Xingyu Zhu², Jiansen He², Jun Cui¹, Hairong Lai¹, Daniel Verscharen^{3,4}, and Die Duan²

¹ School of Atmospheric Sciences, Sun Yat-sen University, Zhuhai, 519000, People's Republic of China; cuijun7@mail.sysu.edu.cn, laihr@mail.sysu.edu.cn

² School of Earth and Space Sciences, Peking University, Beijing 100871, Beijing, People's Republic of China; jshept@pku.edu.cn

³ Mullard Space Science Laboratory, University College London, Dorking, RH5 6NT, UK

⁴ Space Science Center, University of New Hampshire, Durham, NH 03824, USA

Received 2021 October 23; revised 2022 January 29; accepted 2022 February 5; published 2022 March 24

Abstract

Ion cyclotron resonance is one of the fundamental energy-conversion processes through field–particle interaction in collisionless plasmas. However, the key evidence for ion cyclotron resonance (i.e., the coherence between electromagnetic fields and the ion phase-space density) and the resulting damping of ion cyclotron waves (ICWs) has not yet been directly observed. Investigating the high-quality measurements of space plasmas by the Magnetospheric Multiscale (MMS) satellites, we find that both the wave electromagnetic field vectors and the bulk velocity of the disturbed ion velocity distribution rotate around the background magnetic field. Moreover, we find that the absolute gyrophase angle difference between the center of the fluctuations in the ion velocity distribution functions and the wave electric field vectors falls in the range of $(0, 90)^\circ$, consistent with an ongoing energy conversion from wave fields to particles. By invoking plasma kinetic theory, we demonstrate that the field–particle correlation for the damped ICWs in our theoretical model matches well with our observations. Furthermore, the wave electric field vectors ($\delta E'_{\text{wave},\perp}$), ion current density ($\delta J_{i,\perp}$), and energy transfer rate ($\delta J_{i,\perp} \cdot \delta E'_{\text{wave},\perp}$) exhibit quasiperiodic oscillations, and the integrated work done by the electromagnetic field on the ions is positive, indicating that ions are mainly energized by the perpendicular component of the electric field via cyclotron resonance. Therefore, our combined analysis of MMS observations and kinetic theory provides direct, thorough, and comprehensive evidence for ICW damping in space plasmas.

Unified Astronomy Thesaurus concepts: [Space plasmas \(1544\)](#); [Alfven waves \(23\)](#); [Plasma physics \(2089\)](#)

1. Introduction

Ion cyclotron waves (ICWs) are a prevalent phenomenon in various plasma environments, e.g., the Earth's magnetosphere, the magnetosheath, and the solar wind (Anderson et al. 1992; Dunlop et al. 2002; Jian et al. 2009; He et al. 2011; Usanova et al. 2012; Wicks et al. 2016; Zhao et al. 2018, 2019; Telloni et al. 2019; Woodham et al. 2019; Bowen et al. 2020). ICWs near the ion cyclotron frequency can have a close coupling with ions through cyclotron resonance. They are regarded as one of the crucial wave modes in shaping the particle kinetics locally (plasma ions and energetic electrons) and even the dynamics of the global magnetospheric system (Thorne 2010; Su et al. 2014; Yuan et al. 2014). ICWs can have different wave bands corresponding to the cyclotron frequencies of different ion species (e.g., H^+ , He^+ , O^+) and, in the magnetospheric context, may be located in different regions in terms of L-shell and magnetic local time (Allen et al. 2015; Wang et al. 2017). In the Earth's magnetosphere, ICWs can be generated by temperature-anisotropy instabilities through releasing the excess of the ion perpendicular thermal energy, in which case the wave amplitude saturates when the ion thermal anisotropy approaches an equilibrium state. It is widely believed that ICWs cause precipitation of relativistic electrons and energetic ions from the magnetosphere down to the ionosphere and atmosphere through pitch-angle scattering (Hendry et al. 2016; Zhang et al. 2016; Kurita et al. 2018; Qin et al. 2018),

contributing to the decay phase of geomagnetic storms (Jordanova et al. 2006). ICWs can also be damped by converting energy from waves to particles. For example, ICWs can accelerate ions through cyclotron resonance in the polar region, leading to the loss of O^+ from the Earth's atmosphere (Chang et al. 1986), or heat thermal ions preferentially in the direction perpendicular to the background field (Marsch 2006). Quantification of the wave–particle interactions and the association of energy transfer between waves and particles is necessary to better understand critical space plasma phenomena such as ion kinetic physics, particle precipitation, atmospheric loss processes, and the evolution of geomagnetic storms.

Identifying the resonance mechanisms that convert energy between electromagnetic fields and charged particles in nearly collisionless plasmas is a critical step to understand the process of wave–particle interactions (Hollweg & Isenberg 2002; He et al. 2015; Verscharen et al. 2019). He et al. (2015) revealed the coexistence of two wave modes (quasi-parallel ICWs and quasi-perpendicular kinetic Alfvén waves, KAWs) and three resonance diffusion plateaus in proton velocity space, which suggests a complicated scenario of wave–particle interactions in solar wind turbulence: left-handed cyclotron resonance between ICWs and the proton core population and Landau and right-handed cyclotron resonances between KAWs and the proton beam population. According to kinetic theory, ions can be energized by the perpendicular component of the electric field in a subregion of velocity space via cyclotron resonance (Duan et al. 2020; Klein et al. 2020). For the energy transfer via Landau resonance, the field–particle correlation method has been successfully implemented to explore compressive waves in simulations (Klein & Howes 2016; Ruan et al. 2016;

Howes 2018), as well as in observations (Chen et al. 2019). As a pioneering effort of seeking observational evidence for cyclotron resonance, Kitamura et al. (2018) found that the observed ion differential energy flux spectra are not symmetric around the magnetic field direction but are in phase with the plasma wave fields, suggesting that the energy is transferred from ions to ICWs via cyclotron resonance.

The $\mathbf{J} \cdot \mathbf{E}'$ term is often studied in observational time series and simulation data to quantify the energy transfer between fields and particles at various scales (Yang et al. 2017; Chasapis et al. 2018; He et al. 2019, 2020; Duan et al. 2020; Luo et al. 2020). For the interaction between ions and waves, the energy transfer rate is calculated as the dot product of the fluctuating electric field ($\mathbf{E}'_{\text{wave}}$) and the fluctuating ion current (\mathbf{J}_i), both of which are perpendicular to the background magnetic field \mathbf{B}_0 in cyclotron-resonant interactions (Omura et al. 2010). Aside from the $\mathbf{J} \cdot \mathbf{E}'$ term, the term for the pressure-strain tensor interaction, $-(\mathbf{P} \cdot \nabla) \cdot \mathbf{V}$, is another proxy for heating, representing the energy conversion from bulk kinetic energy to thermal energy (Yang et al. 2017; Chasapis et al. 2018; Luo et al. 2020). Simulations suggest that, although scale-dependent, the spatial patterns of $\mathbf{J} \cdot \mathbf{E}'$ and $-(\mathbf{P} \cdot \nabla) \cdot \mathbf{V}$ are often concentrated in proximity to each other (Yang et al. 2019).

However, the field–particle coherent interaction, which is responsible for the damping of ICWs, has not been directly observed. More specifically, the details of the interaction between the electromagnetic field of the ICWs with the fluctuating ion velocity distribution function ($\delta f_i(\mathbf{V})$) is of great importance for understanding field–particle interactions. Here we present the first observation of the correlation between the ion velocity distribution function and the wave electric field vectors elucidating the process of field–particle interaction and the damping process of ICWs.

2. Observations of ICWs and Associated Field–Particle Correlation

We survey the ICW list from the website of the Magnetospheric Multiscale (MMS) science data center⁵ and select the events that were observed in the magnetosphere in burst mode. As a result, we acquire 44 ICW events from 2018 October 15 to 2021 March 13. We find ICW growth in 17 of the 44 events and ICW damping in 16 of the 44 events. The remaining 11 events have no clear signal of ICW growth or damping. Since the growth of these listed ICWs has been studied in depth before (e.g., Kitamura et al. 2018), here we focus on the damping of ICWs. The event, which has typical and clear coherent coupling features between fields and particles, is selected in this study for detailed analysis. It was encountered on 2018 November 1 at 16:39:03 UT–16:39:52 UT, when the MMS spacecraft (Burch et al. 2016) were in the Earth’s outer magnetosphere and near the magnetopause (Figure 1(a)). We use data from the magnetometer at 128 samples s^{-1} (Fluxgate Magnetometer; Russell et al. 2016) and the Fast Plasma Investigation (FPI; Pollock et al. 2016) at 150 ms for ions. By employing the singular value decomposition of the electromagnetic spectral matrix according to Gauss’s and Faraday’s laws (Santolík et al. 2003), we find that the fluctuations are left-hand circularly polarized about the local mean magnetic field direction ($\mathbf{B}_{0,\text{local}}$) and propagate antiparallel to $\mathbf{B}_{0,\text{local}}$

(Figures 1(b)–(c)), strongly suggesting their nature as ICWs. In this ICW event, since the period of ICWs is ~ 4 s, only the time resolution of burst intervals in the magnetic field (128 samples s^{-1}) and ion (150 ms) measurements can meet the needs of analysis. Since burst mode data of the magnetic field and particles are unavailable before and after the interval between 16:39:03 UT and 16:39:52 UT, we choose the time period from 16:39:03 UT to 16:39:52 UT on 2018 November 1 for further analysis.

We use the background magnetic field (\mathbf{B}_0 , i.e., the magnetic field averaged over the full time interval) to define the magnetic field-aligned coordinates. The subscript $\perp 2$ denotes the $\mathbf{B}_0 \times \mathbf{V}_0$ direction (where \mathbf{V}_0 is the velocity averaged over the full time interval), and the subscript $\perp 1$ completes the right-handed system. In Figures 1(d) and (e), the positive correlation between the B -component $B_{\perp 1}(B_{\perp 2})$ and the V -component $V_{i,\perp 1}(V_{i,\perp 2})$ indicates an antiparallel propagation of ICWs. In Figure 1(f), the phase of $V_{i,\perp 2}$ is 90° ahead of $V_{i,\perp 1}$, indicating the left-hand polarization of the wave mode. The temperature of the ions (Figure 1(g)) shows a thermal anisotropy, with $T_{i,\perp}/T_{i,\parallel} = 1.83$.

In Figure 2, the power spectral densities (PSDs) of ion (proton) bulk/fluid velocity (Figures 2(a)–(c)), the magnetic field (Figures 2(d)–(f)), and the electric field (Figures 2(g)–(i)), as well as the spectra of the energy transfer rate (Figures 2(j)–(l)), show peaks around 0.25 Hz. Hence, we define the wave magnetic field ($\delta \mathbf{B}_{\text{wave}}$) as the magnetic field in the frequency range of 0.1–0.5 Hz and obtain the wave magnetic field through filtering with the inverse fast Fourier transform. The components of \mathbf{V}_i in the frequency range of 0.1–0.5 Hz ($\delta \mathbf{V}_{i,\text{wave}}$) are filtered in the same way as $\delta \mathbf{B}_{\text{wave}}$. The filtered wave electric field vectors ($\delta \mathbf{E}'_{\text{wave}}$) in the plasma frame, which moves with the mean flow velocity, are plotted in Figure 1(h), and the phase of $\delta \mathbf{E}'_{\text{wave},\perp 2}$ is 90° ahead of $\delta \mathbf{E}'_{\text{wave},\perp 1}$. In Figure 1, the time series of the magnetic field and fluid velocity are the original measurements, while the wave electric field components and wave ion current density components are filtered in the frequency range of 0.1–0.5 Hz.

The energy transfer rate via cyclotron-resonant interactions between ICWs and ions is calculated as the dot product of $\delta \mathbf{E}'_{\text{wave}}$ and the fluctuating ion current density ($\delta \mathbf{J}_i$) perpendicular to \mathbf{B}_0 . The contributions to the total current density from the ion species are calculated as $\mathbf{J}_i = N_i \cdot q_i \cdot \mathbf{V}_i$ (N_i is the ion’s number density, q_i is the ion’s charge, and \mathbf{V}_i is the ion’s bulk velocity), and the filtered fluctuating ion current density ($\delta \mathbf{J}_i$) is plotted in Figure 1(i). The work done by the electromagnetic field on the ions in the perpendicular directions is illustrated in Figure 1(j). Lastly, the integrated work done by the electromagnetic field on the ions is shown in Figure 1(k). We note that the wave electric field vectors ($\delta \mathbf{E}'_{\text{wave},\perp}$), ion current density ($\delta \mathbf{J}_{i,\perp}$), and energy transfer rate ($\delta \mathbf{J}_{i,\perp} \cdot \delta \mathbf{E}'_{\text{wave},\perp}$) exhibit quasiperiodic oscillations. Positive $\delta \mathbf{J}_{i,\perp} \cdot \delta \mathbf{E}'_{\text{wave},\perp}$ indicates that ions are mainly energized by the perpendicular component of the electric field via cyclotron resonance. In this event, the trend of B_z is similar to the trend of the time-integrated work done by the wave electric field on the ions in the perpendicular direction. Moreover, our interpretation of an active wave–particle interaction also requires certain phase relations between the electric field and the fluctuations in the particle distribution. If we reverse the time series and conduct the same analysis on the new time series, we find that the time-integrated work still has an increasing trend, while the trend of B_z is

⁵ <https://lasp.colorado.edu/mms/sdc/public/>

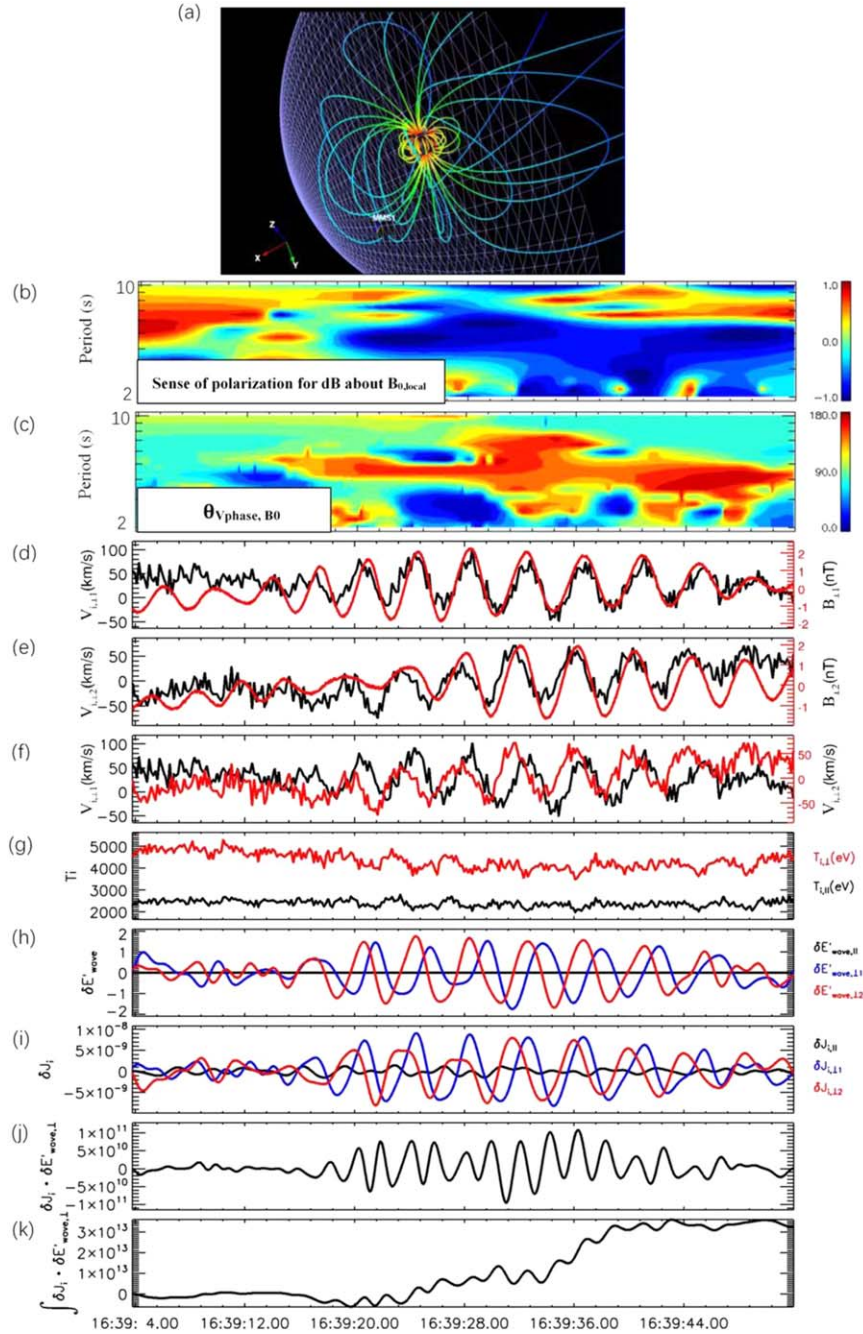


Figure 1. Alfvénic cyclotron waves in the Earth’s outer magnetosphere near the magnetopause as measured by MMS on 2018 November 1. (a) Position of MMS in the outer magnetosphere during the measurement. It is located inside the magnetopause. (b) Sense of polarization for $\delta\mathbf{B}_\perp$ around the local mean magnetic field direction $\mathbf{B}_{0,\text{local}}$, with values of -1 and $+1$ representing the left- and right-hand circular polarization about $\mathbf{B}_{0,\text{local}}$. (c) Angle of propagation direction for electromagnetic field fluctuations with respect to $\mathbf{B}_{0,\text{local}}$, $\theta_{V\text{phase}, B_0}$. (d)–(f) Time series of magnetic field components ($B_{\perp 1}$ and $B_{\perp 2}$), as well as ion (proton) bulk/fluid velocity components ($V_{i,\perp 1}$ and $V_{i,\perp 2}$) in field-aligned coordinates. The positive correlation between the \mathbf{B} and \mathbf{V} components indicates an antiparallel propagation of ICWs. The phase of $V_{i,\perp 1}$ is 90° ahead of $V_{i,\perp 2}$, indicating their left-hand polarization. (g) Parallel and perpendicular temperatures of protons. (h) and (i) Wave electric field and wave ion current density components. (j) Work done by the wave electric fields on the ions in the perpendicular direction. (k) Time-integrated work done by the wave electric field on the ions in the perpendicular direction.

decreasing, which furthermore suggests an active wave-particle interaction.

First-order left-hand cyclotron resonance occurs when the resonance condition $\omega - k_\parallel V_\parallel = n\Omega_i$ is satisfied with $n = 1$, where ω is the wave frequency in the plasma frame, k_\parallel is the wavenumber component parallel to \mathbf{B}_0 , V_\parallel is the parallel particle velocity component, Ω_i is the proton cyclotron frequency, and $n \neq 0$ is the integer resonance number. For the MMS observation considered here, because the ICWs

propagate antiparallel to \mathbf{B}_0 and the frequency of ICWs ($\omega \sim 1.28 \text{ rad s}^{-1}$) is smaller than the proton gyrofrequency ($\Omega_i = 3.57 \text{ rad s}^{-1}$), the resonance condition is satisfied for ions with pitch angles smaller than 90° .

The correlation between the azimuthal angle of the center of the fluctuating ion phase-space density $\phi(\delta f_i(t))$ and the azimuthal angle of the wave electric field vectors $\phi(\delta E'_{\text{wave},\perp}(t))$ is shown in Figures 3(a)–(d). Figures 3(a)–(d) illustrate the $(t-\phi)$ diagrams of the fluctuating ion phase-space

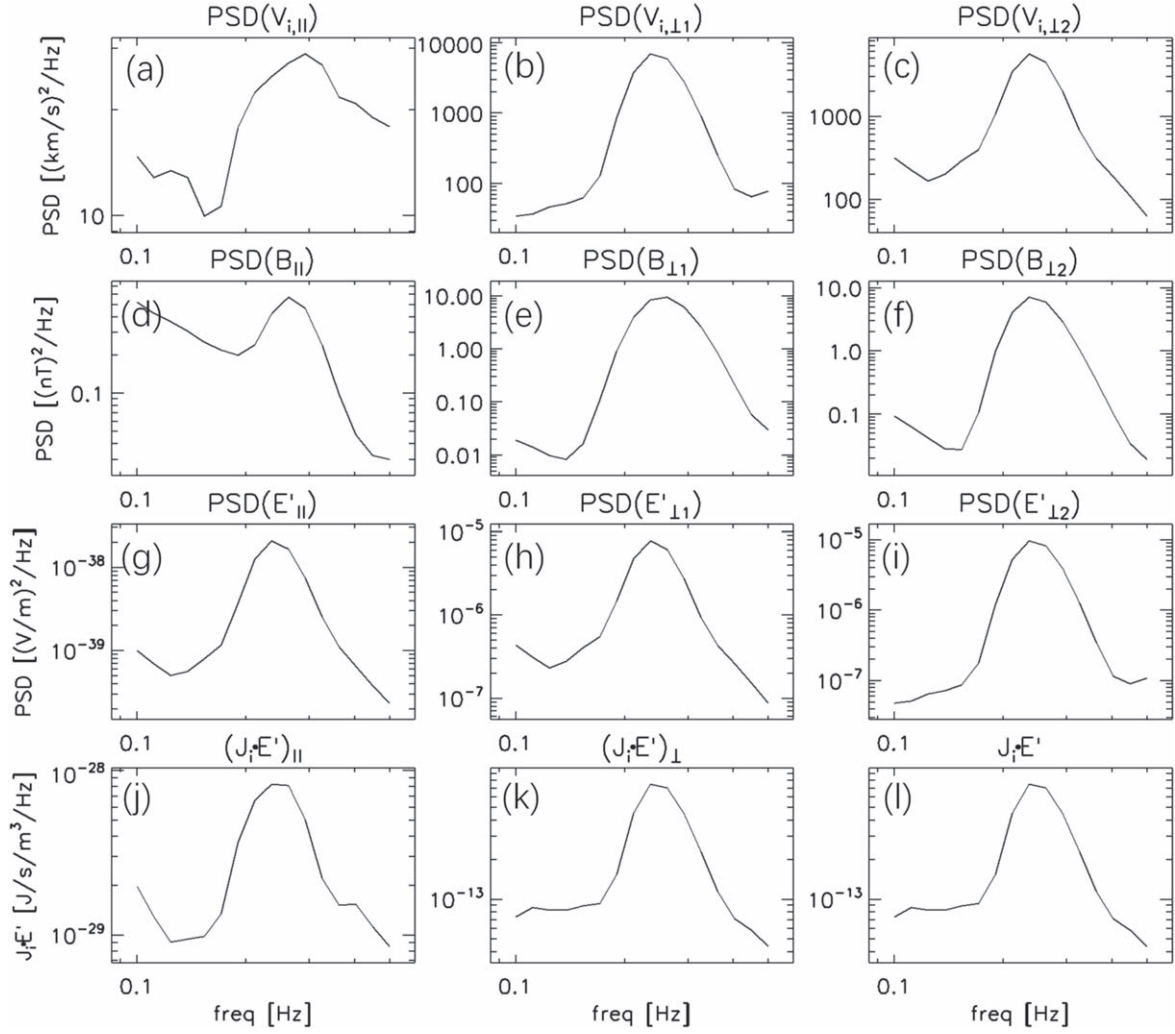


Figure 2. (a)–(c) The PSD of ion (proton) bulk/fluid velocity components ($V_{i,||}$, $V_{i,\perp 1}$, and $V_{i,\perp 2}$) in field-aligned coordinates. (d)–(f) The PSD of magnetic field components ($B_{||}$, $B_{\perp 1}$, and $B_{\perp 2}$) in field-aligned coordinates. (g)–(i) The PSD of electric field components ($E'_{||}$, $E'_{\perp 1}$, and $E'_{\perp 2}$) in field-aligned coordinates. (j)–(l) Spectrum of the energy transfer rate ($(\mathbf{J}_i \cdot \mathbf{E}')_{||}$, $(\mathbf{J}_i \cdot \mathbf{E}')_{\perp}$, and $\mathbf{J}_i \cdot \mathbf{E}'$) in field-aligned coordinates.

density ($\delta f_i = f_i - \langle f_i \rangle$, where $\langle f_i \rangle$ is the time average of the ion phase-space densities) at energies from 2 to 17,013 eV and pitch angles from 2° to 87° as the background. We then superpose the time series of $\phi(\delta \mathbf{E}'_{\text{wave},\perp}(t))$ on them. In other words, from 16:39:18 to 16:39:46, the observed ion velocity distributions are not symmetric around the magnetic field direction but are in phase with the plasma wave fields. Moreover, the absolute angle difference between the azimuthal angle of the fluctuating ion phase-space density $\phi(\delta f_i(t))$, which can be approximated with the angle of the time-dependent local maximum ϕ^* satisfying $\delta f_i(t, \phi^*) = \delta f_{i,\text{max}}(t)$, and the azimuth angle of the wave electric field vectors $\phi(\delta \mathbf{E}'_{\text{wave},\perp}(t))$ is less than 90° . Such a positive correlation between $\phi(\delta \mathbf{E}'_{\text{wave},\perp}(t))$ and $\phi(\delta f_i(t))$ is consistent with positive work done by the electromagnetic field in Figure 1 from 16:39:18 to 16:39:46.

To investigate the damping cyclotron resonance during the interval of [16:39:18, 16:39:46] in more detail, we sort the data of the ion phase-space density according to the relative phase angle (ζ), which is defined as the azimuthal angle difference between $\phi(\delta f_{i,\text{max}})$ and $\phi(\delta \mathbf{E}'_{\text{wave},\perp})$ to represent the gyrophase difference $\delta f_{i,\text{max}}$ relative to the rotating $\delta \mathbf{E}'_{\text{wave},\perp}$. The normalized ion phase-space densities as functions of the relative phase

angle (ζ) averaged over the time duration of 28 s are shown in Figure 3(e), where a significant peak around $\zeta = -75^\circ$ can be identified at all energies. Again, the absolute relative phase angle $|\zeta| = 75^\circ$ is less than 90° , clearly suggesting an ongoing energy transfer from fields to particles and the damping of wave electromagnetic field energy.

3. Comparison of Field–Particle Correlation between Observation and Theory

To compare with the observational results, we investigate the field–particle correlation of ICWs based on linear plasma wave theory (Stix 1992) using our newly developed solver for the full set of perturbations of the linear plasma eigenmodes (Plasma Kinetics Unified Eigenmode Solutions, PKUES). The first part of PKUES is inherited from the solver Plasma Dispersion Relation Kinetics (Xie & Xiao 2016) and calculates all possible eigenmode solutions at a time. Furthermore, like NHDS (Verscharen & Chandran 2018), PKUES provides a full set of characteristic fluctuations (including $\delta \mathbf{B}$, $\delta \mathbf{E}$, δf_i , δf_e , δN_i , $\delta \mathbf{V}_i$, and $\delta \mathbf{V}_e$) for the eigenmode under study. By applying the observed plasma conditions to PKUES, we calculate the coherent fluctuating phase-space density of the specific mode as a function of time and illustrate it in Figure 4 after adding the

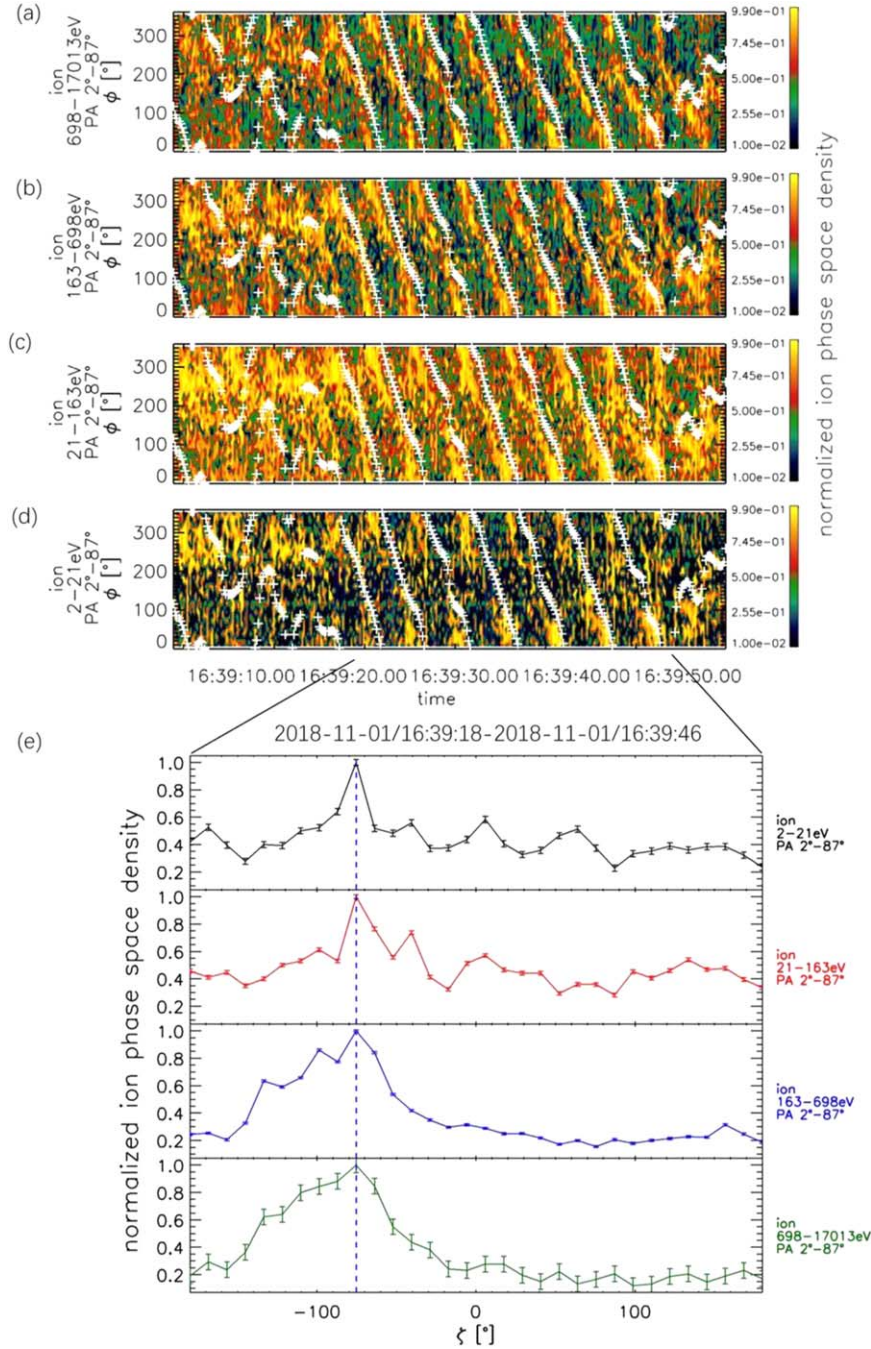


Figure 3. (a)–(d) Correlation between the azimuthal angle of the center of the fluctuating ion phase-space density $\phi(\delta f_i(t))$, which can be approximated with the angle of the time-dependent local maximum $\delta f_i(t, \phi)$, and the azimuthal angle of the wave electric field vectors $\delta E'_{\text{wave},\perp}$ (white plus signs). The observed ion distributions are not symmetric around the magnetic field direction but are in phase with the plasma wave fields. (e) Relative phase-angle (ζ ; i.e., the gyrophase relative to the rotating $\delta E'_{\text{wave},\perp}$) distributions of the 28 s averaged (from 16:39:18 to 16:39:46) ion phase-space densities with the error bars (σ) representing twice the standard error of the mean at every angular bin. Here $\sigma = \sqrt{\sum_{i=1}^n (f_i(t, \zeta) - \langle f(t, \zeta) \rangle)^2 / n}$, where $n = 7$ is the number of wave periods from 16:39:18 to 16:39:46; $f_i(t, \zeta)$ is the average ion phase density in the i th period, and $\langle f(t, \zeta) \rangle$ is the average ion phase density of our seven periods. The blue dashed vertical line in Figure 3(e) denotes the normalized ion phase-space density peak around $\zeta = -75^\circ$.

background bi-Maxwellian distribution. The magnetized plasma parameters used in PKUES are $n_{e0} = n_{p0} = 1.1 \text{ cm}^3$, $T_{\text{pi}} = 2383.3 \text{ eV}$, $T_{\text{ei}} = 348.0 \text{ eV}$, $T_{\text{p}\perp} = 4340.6 \text{ eV}$, $T_{\text{e}\perp} = 458.3 \text{ eV}$, and $v_{\text{d,e}} = v_{\text{d,i}} = 0 \text{ km s}^{-1}$. The theoretically predicted azimuthal angle correlation between the fluctuating ion phase-space density ($\delta f_i(t)$) and the wave electric field vectors ($\delta E'_{\text{wave},\perp}(t)$) also suggests a field-to-particle energy transfer as we observe in Figure 3. Likewise, the relative phase-angle (ζ)

distributions of the theoretically predicted ion phase-space densities are shown in Figure 4(e). We observe a peak around $\zeta = -75^\circ$ located between $[-90, 0]^\circ$ in Figure 4(e), demonstrating that a cyclotron resonance transfers energy from the waves to the ions.

In Figures 5 and 6, we illustrate how the ICW's electromagnetic field vectors ($\delta E'_{\text{wave},\perp}$ and $\delta B_{\text{wave},\perp}$) correlate with the fluctuating ion velocity distribution function ($\delta f_i(V)$). Here

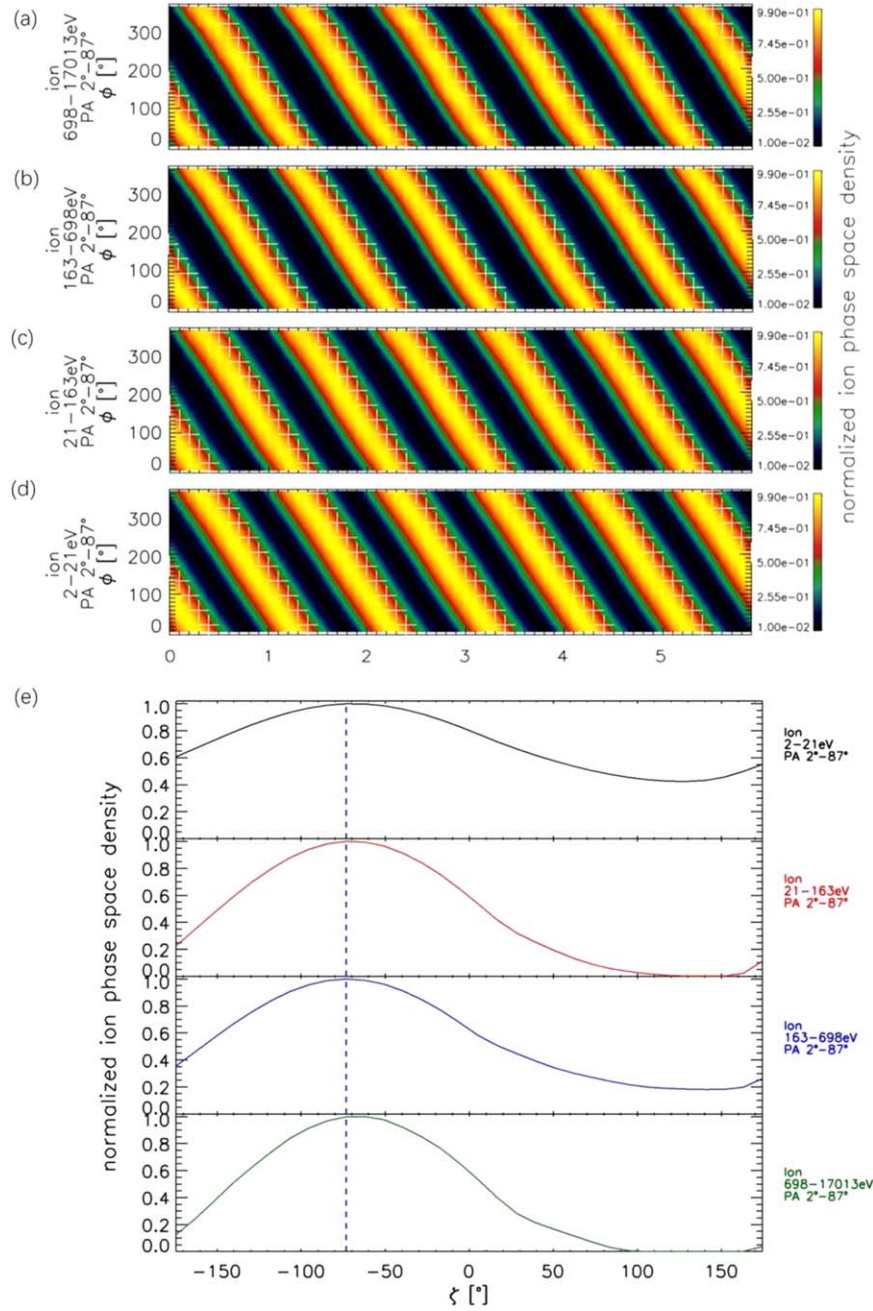


Figure 4. (a)–(d) Correlation between the azimuthal angle of the center of the fluctuating ion phase-space density $\phi(\delta f_i(t))$, the proxy to which can be the angle of the time-dependent local maximum of $\delta f_i(t, \phi)$, and the azimuthal angle of the wave electric field vector $\delta \mathbf{E}'_{\text{wave}, \perp}$, based on the plasma wave prediction from the PKUES solver. (e) Relative average phase-angle (ζ) distributions of the ion phase-space densities. The blue dashed vertical line in Figure 4(e) denotes the normalized ion phase-space density peak around $\zeta = -75^\circ$.

we focus on the energy transfer from ICWs to the ions, which are recorded at a time cadence of 150 ms, resulting in a total of 327 snapshots of 3D velocity distributions. The fluctuating ion velocity distribution function is calculated as $\delta f_i(\mathbf{V}) = f_i(\mathbf{V}) - \langle f_i(\mathbf{V}) \rangle$, where $\langle f_i(\mathbf{V}) \rangle$ is the average of these 327 3D velocity distributions. We show $\delta f_i(\mathbf{V})$ (blue contour surfaces), $\delta \mathbf{B}_{\text{wave}, \perp}$ (yellow bars), and $\delta \mathbf{E}'_{\text{wave}, \perp}$ (green bars) during the period from 16:39:32.63 to 16:39:35.93 of the ICW event in Figure 5. The central position (i.e., the bulk velocity) of $\delta f_i(\mathbf{V})$ is mostly in phase with $\delta \mathbf{E}'_{\text{wave}, \perp}$, and the angle between them is less than 90° for most of the times shown. The phase relations between

the wave fields and ions demonstrate that the cyclotron resonance transfers energy from the wave fields to the ions.

In Figure 6, the 3D contour surfaces of the fluctuating (opaque) and total (transparent) ion phase-space densities at different phases in one wave period are shown based on the PKUES solver. From Figures 6(a) to (h), the bulk velocity vector of $\delta f_i(\mathbf{V})$ rotates with $\delta \mathbf{E}'_{\text{wave}, \perp}$ in the sense of left-hand polarization. Moreover, the 3D contour of $\delta f_i(\mathbf{V})$ bends toward the direction parallel to $\delta \mathbf{E}'_{\text{wave}, \perp}$. Such a corotation of the agyrotropic $\delta f_i(\mathbf{V})$ with $\delta \mathbf{B}_{\text{wave}, \perp}$ and $\delta \mathbf{E}'_{\text{wave}, \perp}$ illustrates the details of the field–particle interaction process responsible for

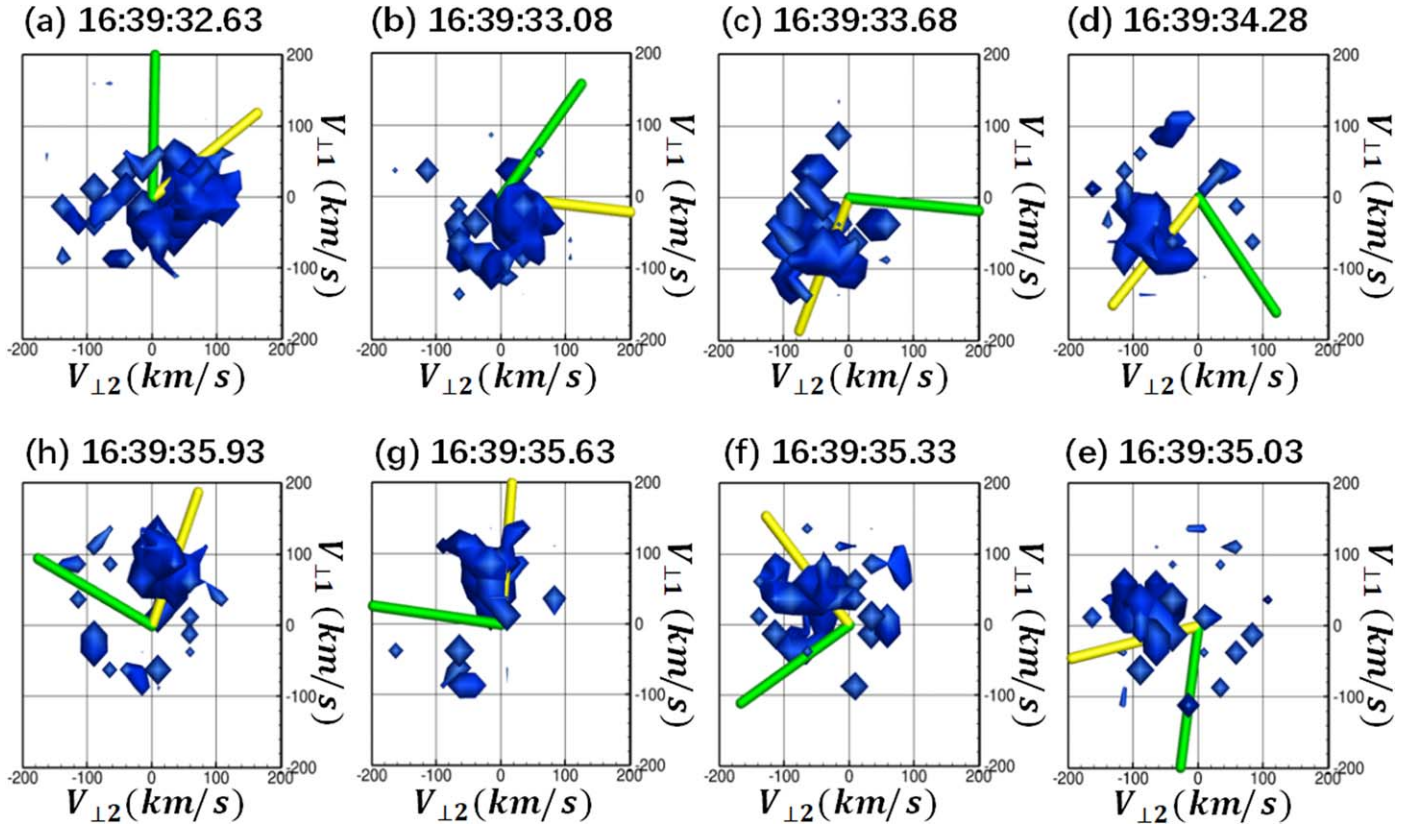


Figure 5. The 3D contour surfaces of the fluctuating ion velocity distribution function ($\delta f_i(V)$) at different phases during one wave period. The contour levels of $\delta f_i(V)$ are selected as $5 \times 10^{-23} \text{ cm}^{-6} \text{ s}^3$. The background magnetic field is in the out-of-plane direction. The wave electric and magnetic field vectors are marked by the green and yellow bars, respectively.

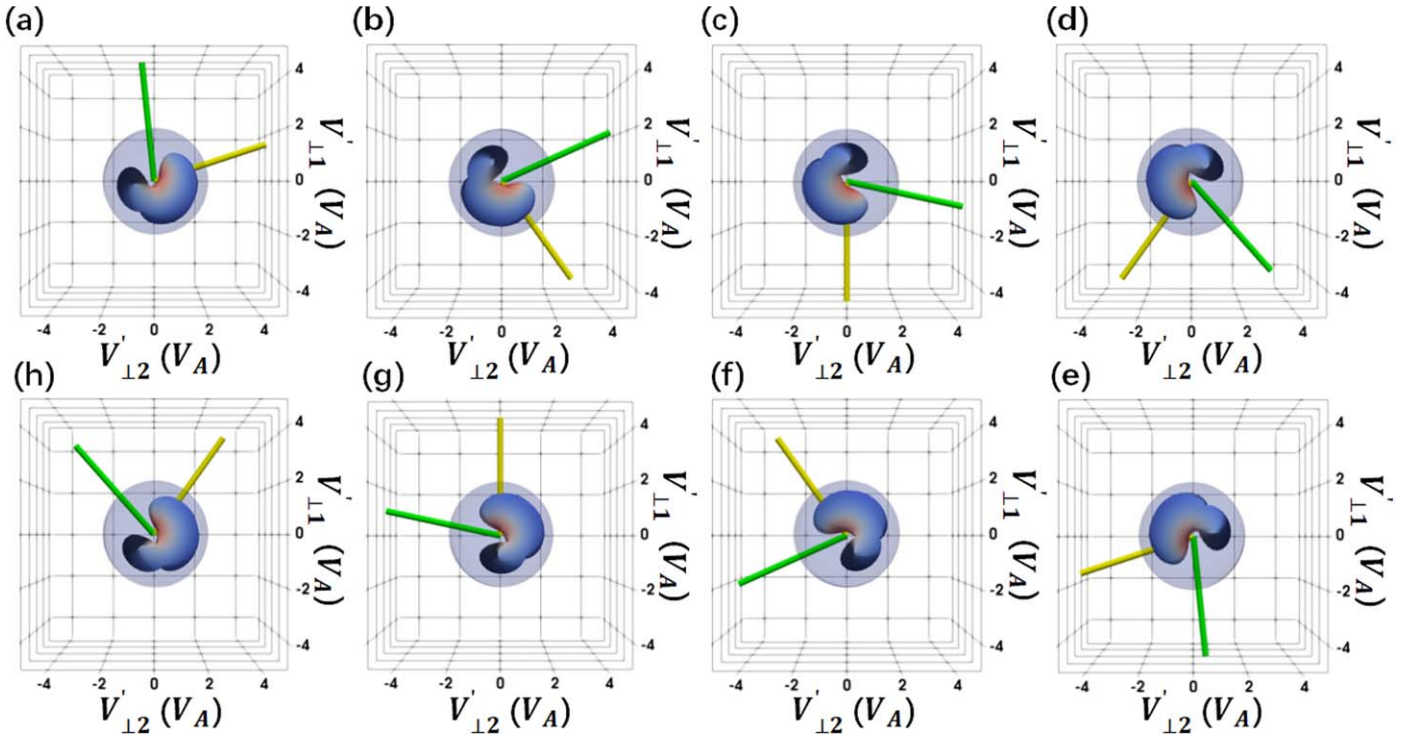


Figure 6. The 3D contour surfaces of the fluctuating (opaque, $\delta f_i(V)$) and total (transparent, $f_i(V)$) ion phase-space density at different phases during one wave period based on the PKUES solver. The contour levels of $\delta f_i(V)$ and $f_i(V)$ are selected as 5×10^{-23} and $5 \times 10^{-24} \text{ cm}^{-6} \text{ s}^3$, respectively. The background magnetic field is in the out-of-plane direction. The green and yellow bars mark the electric and magnetic field vectors, respectively.

the energy conversion from waves to ions. The positive correlation in phase between the bulk velocity vector of $\delta f_i(\mathbf{V})$ and $\delta \mathbf{B}_{\text{wave},\perp}$ in Figures 5 and 6 is consistent with the antiparallel propagation of the analyzed ICWs.

4. Summary and Discussion






Using MMS's measurements of particles and fields, we present the correlation between the fluctuating ion velocity distribution function ($\delta f_i(\mathbf{V})$) and wave electric field vectors $\delta \mathbf{E}'_{\text{wave},\perp}$, which is the essence of cyclotron resonance. The absolute relative phase angle, defined as the azimuthal angle difference between the maximum of $\delta f_i (= \delta f_{i,\text{max}})$ and $\delta \mathbf{E}'_{\text{wave},\perp}$, $|\zeta| = |\phi(\delta f_{i,\text{max}}) - \phi(\delta \mathbf{E}'_{\text{wave},\perp})|$, is less than 90° , suggesting the energy conversion from wave fields to particles. Furthermore, the integrated work done by the electromagnetic field on ions is positive, indicating that ions are mainly energized by the perpendicular component of the electric field via cyclotron resonance. Therefore, our combined analysis of MMS observations and plasma wave theory provides direct and comprehensive evidence for ICW damping in space plasmas.

Since this work focuses on the kinetic energy conversion in the magnetosphere, the direct finding of ICW damping and thus the energy conversion from wave fields to particles is an important step toward the understanding of energy redistribution through field–particle interaction in collisionless plasma. Based on the fact that field–particle interactions occur widely in the heliosphere, the result of this work is of scientific significance because it provides an observational basis supported by theoretical considerations, as well as a physical scenario for the ICW damping and energy conversion in collisionless plasmas. This work also points out that even advanced plasma detectors like FPI on board MMS need to be further improved to meet the needs of accurate measurement of ion velocity distribution in sparse plasmas like the magnetosphere. For this type of work, the most limiting factor is the geometric factor of the instrument.

The authors are grateful to the teams of the MMS spacecraft for providing the data. We also thank the team of 3DView, which is maintained mainly by IRAP/CNES. The work at Sun Yat-sen University is supported by NSFC through grant 2030201. The work at Peking University is supported by NSFC (Nos. 41874200 and 42174194) and the National Key R&D Program of China (No. 2021YFA0718600). D.V. from UCL is supported by STFC Ernest Rutherford Fellowship ST/P003826/1 and STFC Consolidated Grant ST/S000240/1. This work is also supported by CNSA under contract Nos. D020301 and D020302 and supported by the Key Research Program of the Institute of Geology & Geophysics, CAS, grant IGGCAS-201904. X.Y.Z. is the co-first author of this work.

The source code of “PKUES” can be found at <https://github.com/PKU-Heliosphere/PKUES>.

ORCID iDs

Xingyu Zhu  <https://orcid.org/0000-0002-1541-6397>
 Jiansen He  <https://orcid.org/0000-0001-8179-417X>
 Jun Cui  <https://orcid.org/0000-0002-4721-8184>
 Hairong Lai  <https://orcid.org/0000-0001-5750-7919>
 Daniel Verscharen  <https://orcid.org/0000-0002-0497-1096>

References

- Allen, R. C., Zhang, J. C., Kistler, L. M., et al. 2015, *JGRA*, 120, 5574
 Anderson, B. J., Erlanson, R. E., & Zanetti, L. J. 1992, *JGR*, 97, 3089
 Bowen, T. A., Mallet, A., Huang, J., et al. 2020, *ApJS*, 246, 66
 Burch, J. L., Moore, T. E., Torbert, R. B., & Giles, B. L. 2016, *SSRv*, 199, 5
 Chang, T., Crew, G. B., Hershkowitz, N., et al. 1986, *GeoRL*, 13, 636
 Chasapis, A., Yang, Y., Matthaeus, W. H., et al. 2018, *ApJ*, 862, 32
 Chen, C. H. K., Klein, K. G., & Howes, G. G. 2019, *NatCo*, 10, 740
 Duan, D., He, J., Wu, H., & Verscharen, D. 2020, *ApJ*, 896, 47
 Dunlop, M. W., Lucek, E. A., Kistler, L. M., et al. 2002, *JGRA*, 107, 1228
 He, J., Duan, D., Wang, T., et al. 2019, *ApJ*, 880, 121
 He, J., Marsch, E., Tu, C., Yao, S., & Tian, H. 2011, *ApJ*, 731, 85
 He, J., Wang, L., Tu, C., Marsch, E., & Zong, Q. 2015, *ApJL*, 800, L31
 He, J., Zhu, X., Verscharen, D., et al. 2020, *ApJ*, 898, 43
 Hendry, A. T., Rodger, C. J., Clilverd, M. A., et al. 2016, *JGRA*, 121, 5366
 Hollweg, J. V., & Isenberg, P. A. 2002, *JGRA*, 107, 1147
 Howes, G. G. 2018, *PhPl*, 25, 055501
 Jian, L. K., Russell, C. T., Luhmann, J. G., et al. 2009, *ApJL*, 701, L105
 Jordanova, V. K., Miyoshi, Y. S., Zaharia, S., et al. 2006, *JGRA*, 111, A11S10
 Kitamura, N., Kitahara, M., Shoji, M., et al. 2018, *Sci*, 361, 1000
 Klein, K. G., & Howes, G. G. 2016, *ApJL*, 826, L30
 Klein, K. G., Howes, G. G., TenBarge, J. M., & Valentini, F. 2020, *JPIPh*, 86, 905860402
 Kurita, S., Miyoshi, Y., Shiokawa, K., et al. 2018, *GeoRL*, 45, 720
 Luo, Q., He, J., Cui, J., et al. 2020, *ApJL*, 904, L16
 Marsch, E. 2006, *LRSP*, 3, 1
 Omura, Y., Pickett, J., Grison, B., et al. 2010, *JGRA*, 115, A07234
 Pollock, C., Moore, T., Jacques, A., et al. 2016, *SSRv*, 199, 331
 Qin, M., Hudson, M., Millan, R., Woodger, L., & Shekhar, S. 2018, *JGRA*, 123, 6223
 Ruan, W., He, J., Zhang, L., et al. 2016, *ApJ*, 825, 58
 Russell, C. T., Anderson, B. J., Baumjohann, W., et al. 2016, *SSRv*, 199, 189
 Santolík, O., Aarot, M., & Lefeuvre, F. 2003, *RaSc*, 38, 1010
 Stix, T. H. 1992, *Waves in Plasmas* (New York: AIP)
 Su, Z., Zhu, H., Xiao, F., et al. 2014, *PhPl*, 21, 052310
 Telloni, D., Carbone, F., Bruno, R., et al. 2019, *ApJL*, 885, L5
 Thorne, R. M. 2010, *GeoRL*, 37, L22107
 Usanova, M., Darrouzet, F., Mann, I. R., & Bortnik, J. 2012, AGU Meeting, 2012, SM23E-03
 Verscharen, D., & Chandran, B. D. G. 2018, *RNAAS*, 2, 13
 Verscharen, D., Klein, K. G., & Maruca, B. A. 2019, *LRSP*, 16, 5
 Wang, X. Y., Huang, S. Y., Allen, R. C., et al. 2017, *JGRA*, 122, 8228
 Wicks, R. T., Alexander, R. L., Stevens, M., et al. 2016, *ApJ*, 819, 6
 Woodham, L. D., Wicks, R. T., Verscharen, D., et al. 2019, *ApJL*, 884, L53
 Xie, H., & Xiao, Y. 2016, *PIST*, 18, 97
 Yang, Y., Matthaeus, W. H., Parashar, T. N., et al. 2017, *PhRvE*, 95, 061201
 Yang, Y., Wan, M., Matthaeus, W. H., et al. 2019, *MNRAS*, 482, 4933
 Yuan, Z., Xiong, Y., Huang, S., et al. 2014, *GeoRL*, 41, 1830
 Zhang, J., Halford, A. J., Saikin, A. A., et al. 2016, *JGRA*, 121, 11086
 Zhao, J. S., Wang, T. Y., Dunlop, M. W., et al. 2018, *ApJ*, 867, 58
 Zhao, J. S., Wang, T. Y., Dunlop, M. W., et al. 2019, *GeoRL*, 46, 4545